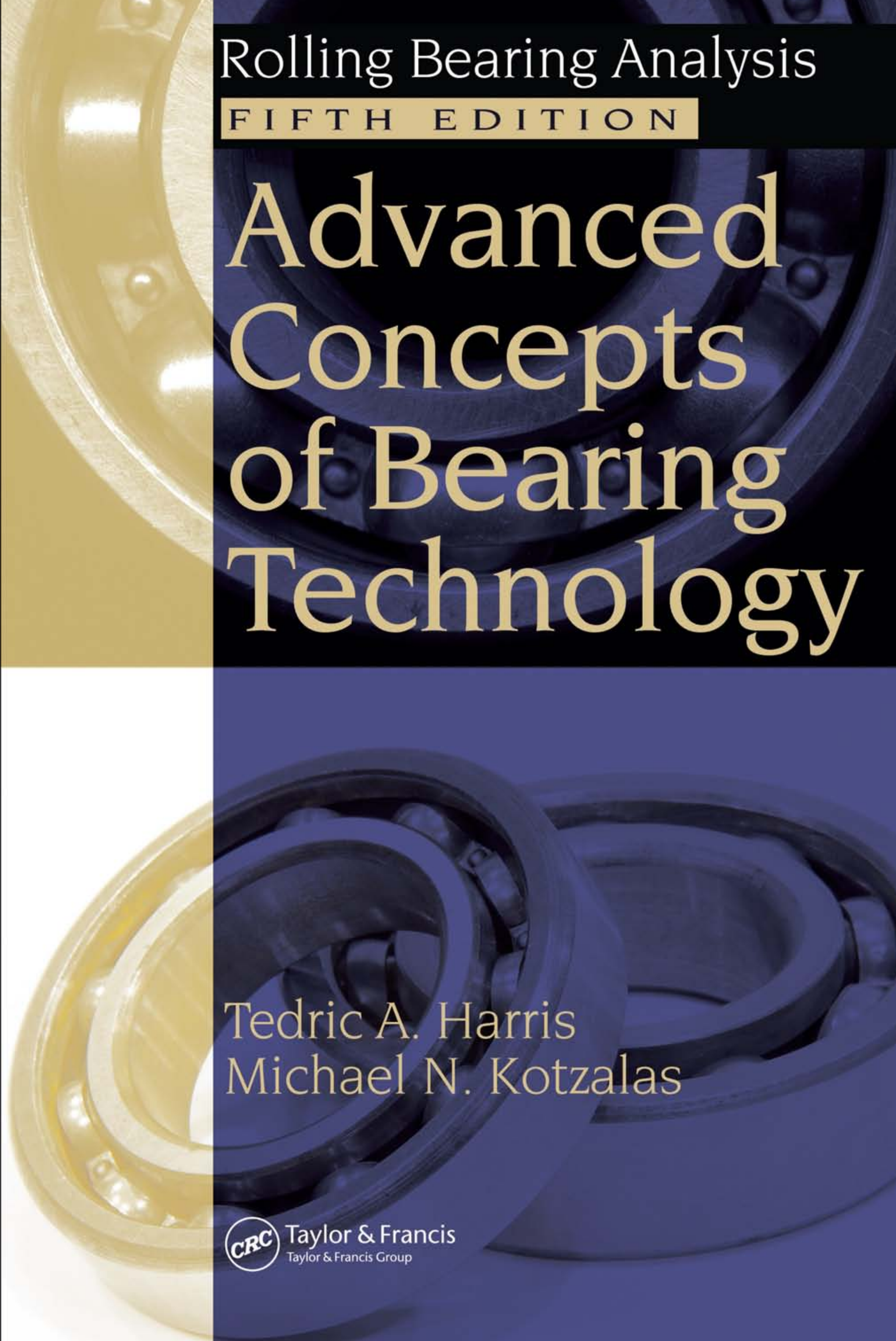

Rolling Bearing Analysis

FIFTH EDITION

# Advanced Concepts of Bearing Technology

Tedric A. Harris
Michael N. Kotzalas

CRC Taylor & Francis
Taylor & Francis Group

Rolling Bearing Analysis

FIFTH EDITION

# Advanced Concepts of Bearing Technology

Rolling Bearing Analysis

FIFTH EDITION

# Advanced Concepts of Bearing Technology

Tedric A. Harris
Michael N. Kotzalas

CRC Taylor & Francis
Taylor & Francis Group
Boca Raton London New York

CRC is an imprint of the Taylor & Francis Group,
an informa business

CRC Press
Taylor & Francis Group
6000 Broken Sound Parkway NW, Suite 300
Boca Raton, FL 33487-2742


Printed in the United States of America on acid-free paper
10 9 8 7 6 5 4 3 2 1

International Standard Book Number-10: 0-8493-7182-1 (Hardcover)
International Standard Book Number-13: 978-0-8493-7182-0 (Hardcover)



**Visit the Taylor & Francis Web site at**
**http://www.taylorandfrancis.com**

**and the CRC Press Web site at**
**http://www.crcpress.com**

# Preface

The main purpose of the first volume of this handbook was to provide the reader with information on the use, design, and performance of ball and roller bearings in common and relatively noncomplex applications. Such applications generally involve slow-to-moderate speed, shaft, or bearing outer ring rotation; simple, statically applied, radial or thrust loading; bearing mounting that does not include misalignment of shaft and bearing outer-ring axes; and adequate lubrication. These applications are generally covered by the engineering information provided in the catalogs supplied by the bearing manufacturers. While catalog information is sufficient to enable the use of the manufacturer's product, it is always empirical in nature and rarely provides information on the geometrical and physical justifications of the engineering formulas cited. The first volume not only includes the underlying mathematical derivations of many of the catalog-contained formulas, but also provides means for the engineering comparison of rolling bearings of various types and from different manufacturers.

Many modern bearing applications, however, involve machinery operating at high speeds; very heavy combined radial, axial, and moment loadings; high or low temperatures; and otherwise extreme environments. While rolling bearings are capable of operating in such environments, to assure adequate endurance, it is necessary to conduct more sophisticated engineering analyses of their performance than can be achieved using the methods and formulas provided in the first volume of this handbook. This is the purpose of the present volume.

When compared with its earlier editions, this edition presents updated and more accurate information to estimate rolling contact friction shear stresses and their effects on bearing functional performance and endurance. Also, means are included to calculate the effects on fatigue endurance of all stresses associated with the bearing rolling and sliding contacts. These comprise stresses due to applied loading, bearing mounting, ring speeds, material processing, and particulate contamination.

The breadth of the material covered in this text, for credibility, can hardly be covered by the expertise of the two authors. Therefore, in the preparation of this text, information provided by various experts in the field of ball and roller bearing technology was utilized. Contributions from the following persons are hereby gratefully acknowledged:

| | |
|---|---|
| Neal DesRuisseaux | bearing vibration and noise |
| John I. McCool | bearing statistical analysis |
| Frank R. Morrison | bearing testing |
| Joseph M. Perez | lubricants |
| John R. Rumierz | lubricants and materials |
| Donald R. Wensing | bearing materials |


Finally, since its initial publication in 1967, *Rolling Bearing Analysis* has evolved into this 5th edition. We have endeavored to maintain the material presented in an up-to-date and useful format. We hope that the readers will find this edition as useful as its earlier editions.

Tedric A. Harris
Michael N. Kotzalas

# Authors

**Tedric A. Harris** is a graduate in mechanical engineering from the Pennsylvania State University, who received a B.S. in 1953 and an M.S. in 1954. After graduation, he was employed as a development test engineer at the Hamilton Standard Division, United Aircraft Corporation, Windsor Locks, Connecticut, and later as an analytical design engineer at the Bettis Atomic Power Laboratory, Westinghouse Electric Corporation, Pittsburgh, Pennsylvania. In 1960, he joined SKF Industries, Inc. in Philadelphia, Pennsylvania as a staff engineer. At SKF, Harris held several key management positions: manager, analytical services; director, corporate data systems; general manager, specialty bearings division; vice president, product technology & quality; president, SKF Tribonetics; vice president, engineering & research, MRC Bearings (all in the United States); director for group information systems at SKF headquarters, Gothenburg, Sweden; and managing director of the engineering & research center in the Netherlands. He retired from SKF in 1991 and was appointed as a professor of mechanical engineering at the Pennsylvania State University at University Park. He taught courses in machine design and tribology and conducted research in the field of rolling contact tribology at the university until retirement in 2001. Currently, he is a practicing consulting engineer and, as adjunct professor in mechanical engineering, teaches courses in bearing technology to graduate engineers in the university's continuing education program.

Harris is the author of 67 technical publications, mostly on rolling bearings. Among these is the book *Rolling Bearing Analysis*, currently in its 5th edition. In 1965 and 1968, he received outstanding technical paper awards from the Society of Tribologists and Lubrication Engineers and in 2001 from the American Society of Mechanical Engineers (ASME) Tribology Division. In 2002, he received the outstanding research award from the ASME.

Harris has served actively in numerous technical organizations, including the Anti-Friction Bearing Manufacturers' Association, ASME Tribology Division, and ASME Research Committee on Lubrication. He was elected ASME Fellow Member in 1973. He has served as chair of the ASME Tribology Division and as chair of the Tribology Division's Nominations and Oversight Committee. He holds three U.S. patents.

**Michael N. Kotzalas** graduated from the Pennsylvania State University with a B.S. in 1994, M.S. in 1997, and Ph.D. in 1999, all in mechanical engineering. During this time, the focus of his study and research was on the analysis of rolling bearing technology, including quasidynamic modeling of ball and cylindrical roller bearings for high-acceleration applications and spall progression testing and modeling for use in condition-based maintenance algorithms.

Since graduation, Dr. Kotzalas has been employed by The Timken Company in research and development and most recently in the industrial bearing business. His current responsibilities include advanced product design and application support for industrial bearing customers, while the previous job profile in research and development included new product and analysis algorithm development. From these studies, Dr. Kotzalas has received two U.S. patents for cylindrical roller bearing designs.

Outside of work, Dr. Kotzalas is also an active member of many industrial societies. As a member of the ASME, he currently serves as the chair of the publications committee and as a member of the rolling element bearing technical committee. He is a member of the awards committee in the Society of Tribologists and Lubrication Engineers (STLE). Dr. Kotzalas has also published ten articles in peer-reviewed journals and one conference proceeding. Some of his publications were honored with the ASME Tribology Division's Best Paper Award in 2001 and STLE's Hodson Award in 2003 and 2006. Also, working with the American Bearing Manufacturer's Association (ABMA), Dr. Kotzalas is one of the many instructors for the short course "Advanced Concepts of Bearing Technology".

# Table of Contents

**Chapter 1**
Distribution of Internal Loading in Statically Loaded Bearings: Combined Radial, Axial, and Moment Loadings—Flexible Support of Bearing Rings ........ 1
1.1 General ........ 2
1.2 Ball Bearings under Combined Radial, Thrust, and Moment Loads ........ 3
1.3 Misalignment of Radial Roller Bearings ........ 8
1.3.1 Components of Deformation ........ 8
1.3.1.1 Crowning ........ 9
1.3.2 Load on a Roller–Raceway Contact Lamina ........ 13
1.3.3 Equations of Static Equilibrium ........ 14
1.3.4 Deflection Equations ........ 15
1.4 Thrust Loading of Radial Cylindrical Roller Bearings ........ 17
1.4.1 Equilibrium Equations ........ 20
1.4.2 Deflection Equations ........ 21
1.4.3 Roller–Raceway Deformations Due to Skewing ........ 22
1.5 Radial, Thrust, and Moment Loadings of Radial Roller Bearings ........ 24
1.5.1 Cylindrical Roller Bearings ........ 24
1.5.2 Tapered Roller Bearings ........ 25
1.5.3 Spherical Roller Bearings ........ 26
1.6 Stresses in Roller–Raceway Nonideal Line Contacts ........ 26
1.7 Flexibly Supported Rolling Bearings ........ 28
1.7.1 Ring Deflections ........ 28
1.7.2 Relative Radial Approach of Rolling Elements to the Ring ........ 34
1.7.3 Determination of Rolling Element Loads ........ 35
1.7.4 Finite Element Methods ........ 37
1.8 Closure ........ 39
References ........ 39

**Chapter 2**
Bearing Component Motions and Speeds ........ 41
2.1 General ........ 42
2.2 Rolling and Sliding ........ 42
2.2.1 Geometrical Considerations ........ 42
2.2.2 Sliding and Deformation ........ 44
2.3 Orbital, Pivotal, and Spinning Motions in Ball Bearings ........ 46
2.3.1 General Motions ........ 46
2.3.2 No Gyroscopic Pivotal Motion ........ 51
2.3.3 Spin-to-Roll Ratio ........ 52
2.3.4 Calculation of Rolling and Spinning Speeds ........ 53
2.3.5 Gyroscopic Motion ........ 55
2.4 Roller End–Flange Sliding in Roller Bearings ........ 56
2.4.1 Roller End–Flange Contact ........ 56
2.4.2 Roller End–Flange Geometry ........ 56

2.4.3 Sliding Velocity ... 59
2.5 Closure ... 60
References ... 61

**Chapter 3**
High-Speed Operation: Ball and Roller Dynamic Loads and Bearing Internal Load Distribution ... 63
3.1 General ... 64
3.2 Dynamic Loading of Rolling Elements ... 65
3.2.1 Body Forces Due to Rolling Element Rotations ... 65
3.2.2 Centrifugal Force ... 68
3.2.2.1 Rotation about the Bearing Axis ... 68
3.2.2.2 Rotation about an Eccentric Axis ... 73
3.2.3 Gyroscopic Moment ... 74
3.3 High-Speed Ball Bearings ... 75
3.3.1 Ball Excursions ... 83
3.3.2 Lightweight Balls ... 83
3.4 High-Speed Radial Cylindrical Roller Bearings ... 84
3.4.1 Hollow Rollers ... 87
3.5 High-Speed Tapered and Spherical Roller Bearings ... 87
3.6 Five Degrees of Freedom in Loading ... 88
3.7 Closure ... 90
References ... 93

**Chapter 4**
Lubricant Films in Rolling Element–Raceway Contacts ... 95
4.1 General ... 97
4.2 Hydrodynamic Lubrication ... 97
4.2.1 Reynolds Equation ... 97
4.2.2 Film Thickness ... 100
4.2.3 Load Supported by the Lubricant Film ... 101
4.3 Isothermal Elastohydrodynamic Lubrication ... 101
4.3.1 Viscosity Variation with Pressure ... 101
4.3.2 Deformation of Contact Surfaces ... 105
4.3.3 Pressure and Stress Distribution ... 108
4.3.4 Lubricant Film Thickness ... 111
4.4 Very-High-Pressure Effects ... 112
4.5 Inlet Lubricant Frictional Heating Effects ... 113
4.6 Starvation of Lubricant ... 114
4.7 Surface Topography Effects ... 116
4.8 Grease Lubrication ... 118
4.9 Lubrication Regimes ... 121
4.10 Closure ... 123
References ... 123

**Chapter 5**
Friction in Rolling Element–Raceway Contacts ... 127
5.1 General ... 128
5.2 Rolling Friction ... 129
5.2.1 Deformation ... 129
5.2.2 Elastic Hysteresis ... 129

5.3 Sliding Friction ... 130
5.3.1 Microslip ... 130
5.3.2 Sliding Due to Rolling Motion: Solid-Film or Boundary Lubrication ... 132
5.3.2.1 Direction of Sliding ... 132
5.3.2.2 Sliding Friction ... 133
5.3.3 Sliding Due to Rolling Motion: Full Oil-Film Lubrication ... 135
5.3.3.1 Newtonian Lubricant ... 135
5.3.3.2 Lubricant Film Parameter ... 135
5.3.3.3 Non-Newtonian Lubricant in an Elastohydrodynamic Lubrication Contact ... 135
5.3.3.4 Limiting Shear Stress ... 137
5.3.3.5 Fluid Shear Stress for Full-Film Lubrication ... 137
5.3.4 Sliding Due to Rolling Motion: Partial Oil-Film Lubrication ... 138
5.3.4.1 Overall Surface Friction Shear Stress ... 138
5.3.4.2 Friction Force ... 139
5.4 Real Surfaces, Microgeometry, and Microcontacts ... 139
5.4.1 Real Surfaces ... 139
5.4.2 GW Model ... 140
5.4.3 Plastic Contacts ... 143
5.4.4 Application of the GW Model ... 143
5.4.5 Asperity-Supported and Fluid-Supported Loads ... 145
5.4.6 Sliding Due to Rolling Motion: Roller Bearings ... 145
5.4.6.1 Sliding Velocities and Friction Shear Stresses ... 145
5.4.6.2 Contact Friction Force ... 146
5.4.7 Sliding Due to Spinning and Gyroscopic Motions ... 147
5.4.7.1 Sliding Velocities and Friction Shear Stresses ... 147
5.4.7.2 Contact Friction Force Components ... 148
5.4.8 Sliding in a Tilted Roller–Raceway Contact ... 148
5.5 Closure ... 148
References ... 150

**Chapter 6**
Friction Effects in Rolling Bearings ... 153
6.1 General ... 154
6.2 Bearing Friction Sources ... 155
6.2.1 Sliding in Rolling Element–Raceway Contacts ... 155
6.2.2 Viscous Drag on Rolling Elements ... 155
6.2.3 Sliding between the Cage and the Bearing Rings ... 156
6.2.4 Sliding between Rolling Elements and Cage Pockets ... 156
6.2.5 Sliding between Roller Ends and Ring Flanges ... 156
6.2.6 Sliding Friction in Seals ... 158
6.3 Bearing Operation with Solid-Film Lubrication: Effects of Friction Forces and Moments ... 158
6.3.1 Ball Bearings ... 158
6.3.2 Roller Bearings ... 163
6.4 Bearing Operation with Fluid-Film Lubrication: Effects of Friction Forces and Moments ... 166
6.4.1 Ball Bearings ... 166
6.4.1.1 Calculation of Ball Speeds ... 166
6.4.1.2 Skidding ... 170

6.4.2 Cylindrical Roller Bearings ........ 174
6.4.2.1 Calculation of Roller Speeds ........ 174
6.4.2.2 Skidding ........ 176
6.5 Cage Motions and Forces ........ 177
6.5.1 Influence of Speed ........ 177
6.5.2 Forces Acting on the Cage ........ 177
6.5.3 Steady-State Conditions ........ 179
6.5.4 Dynamic Conditions ........ 182
6.6 Roller Skewing ........ 183
6.6.1 Roller Equilibrium Skewing Angle ........ 185
6.7 Closure ........ 188
References ........ 189

**Chapter 7**
Rolling Bearing Temperatures ........ 191
7.1 General ........ 192
7.2 Friction Heat Generation ........ 193
7.2.1 Ball Bearings ........ 193
7.2.2 Roller Bearings ........ 194
7.3 Heat Transfer ........ 196
7.3.1 Modes of Heat Transfer ........ 196
7.3.2 Heat Conduction ........ 196
7.3.3 Heat Convection ........ 196
7.3.4 Heat Radiation ........ 198
7.4 Analysis of Heat Flow ........ 199
7.4.1 Systems of Equations ........ 199
7.4.2 Solution of Equations ........ 201
7.4.3 Temperature Node System ........ 202
7.5 High Temperature Considerations ........ 203
7.5.1 Special Lubricants and Seals ........ 203
7.5.2 Heat Removal ........ 205
7.6 Heat Transfer in a Rolling–Sliding Contact ........ 205
7.7 Closure ........ 208
References ........ 208

**Chapter 8**
Application Load and Life Factors ........ 209
8.1 General ........ 210
8.2 Effect of Bearing Internal Load Distribution on Fatigue Life ........ 211
8.2.1 Ball Bearing Life ........ 211
8.2.1.1 Raceway Life ........ 211
8.2.1.2 Ball Life ........ 212
8.2.2 Roller Bearing Life ........ 213
8.2.2.1 Raceway Life ........ 213
8.2.2.2 Roller Life ........ 213
8.2.3 Clearance ........ 214
8.2.4 Flexibly Supported Bearings ........ 215
8.2.5 High-Speed Operation ........ 215
8.2.6 Misalignment ........ 218
8.3 Effect of Lubrication on Fatigue Life ........ 219
8.4 Effect of Material and Material Processing on Fatigue Life ........ 223

8.5 Effect of Contamination on Fatigue Life ... 224
8.6 Combining Fatigue Life Factors ... 228
8.7 Limitations of the Lundberg–Palmgren Theory ... 231
8.8 Ioannides–Harris Theory ... 234
8.9 The Stress–Life Factor ... 236
8.9.1 Life Equation ... 236
8.9.2 Fatigue-Initiating Stress ... 237
8.9.3 Subsurface Stresses Due to Normal Stresses Acting on the Contact Surfaces ... 237
8.9.4 Subsurface Stresses Due to Frictional Shear Stresses Acting on the Contact Surfaces ... 238
8.9.5 Stress Concentration Associated with Surface Friction Shear Stress ... 238
8.9.6 Stresses Due to Particulate Contaminants ... 240
8.9.7 Combination of Stress Concentration Factors Due to Lubrication and Contamination ... 247
8.9.8 Effect of Lubricant Additives on Bearing Fatigue Life ... 247
8.9.9 Hoop Stresses ... 247
8.9.10 Residual Stresses ... 248
8.9.10.1 Sources of Residual Stresses ... 248
8.9.10.2 Alterations of Residual Stress Due to Rolling Contact ... 249
8.9.10.3 Work Hardening ... 250
8.9.11 Life Integral ... 251
8.9.12 Fatigue Limit Stress ... 253
8.9.13 ISO Standard ... 253
8.10 Closure ... 255
References ... 256

**Chapter 9**
Statically Indeterminate Shaft–Bearing Systems ... 259
9.1 General ... 260
9.2 Two-Bearing Systems ... 260
9.2.1 Rigid Shaft Systems ... 260
9.2.2 Flexible Shaft Systems ... 262
9.3 Three-Bearing Systems ... 265
9.3.1 Rigid Shaft Systems ... 265
9.3.2 Nonrigid Shaft Systems ... 266
9.3.2.1 Rigid Shafts ... 269
9.4 Multiple-Bearing Systems ... 270
9.5 Closure ... 272
Reference ... 272

**Chapter 10**
Failure and Damage Modes in Rolling Bearings ... 273
10.1 General ... 273
10.2 Bearing Failure Due to Faulty Lubrication ... 274
10.2.1 Interruption of Lubricant Supply to Bearings ... 274
10.2.2 Thermal Imbalance ... 274
10.3 Fracture of Bearing Rings Due to Fretting ... 276
10.4 Bearing Failure Due to Excessive Thrust Loading ... 279
10.5 Bearing Failure Due to Cage Fracture ... 280

10.6 Incipient Failure Due to Pitting or Indentation of the Rolling Contact Surfaces 283
10.6.1 Corrosion Pitting 283
10.6.2 True Brinnelling 284
10.6.3 False Brinnelling in Bearing Raceways 284
10.6.4 Pitting Due to Electric Current Passing through the Bearing 285
10.6.5 Indentations Caused by Hard Particle Contaminants 285
10.6.6 Effect of Pitting and Denting on Bearing Functional Performance and Endurance 286
10.7 Wear 293
10.7.1 Definition of Wear 293
10.7.2 Types of Wear 294
10.8 Micropitting 295
10.9 Surface-Initiated Fatigue 295
10.10 Subsurface-Initiated Fatigue 300
10.11 Closure 300
References 302

**Chapter 11**
Bearing and Rolling Element Endurance Testing and Analysis 303
11.1 General 304
11.2 Life Testing Problems and Limitations 306
11.2.1 Acceleration of Endurance Testing 306
11.2.2 Acceleration of Endurance Testing through Very Heavy Applied Loading 306
11.2.3 Avoiding Test Operation in the Plastic Deformation Regime 306
11.2.4 Load–Life Relationship of Roller Bearings 307
11.2.5 Acceleration of Endurance Testing through High-Speed Operation 307
11.2.6 Testing in the Marginal Lubrication Regime 308
11.3 Practical Testing Considerations 308
11.3.1 Particulate Contaminants in the Lubricant 308
11.3.2 Moisture in the Lubricant 309
11.3.3 Chemical Composition of the Lubricant 309
11.3.4 Consistency of Test Conditions 309
11.3.4.1 Condition Changes over the Test Period 309
11.3.4.2 Lubricant Property Changes 309
11.3.4.3 Control of Temperature 310
11.3.4.4 Deterioration of Bearing Mounting Hardware 310
11.3.4.5 Failure Detection 310
11.3.4.6 Concurrent Test Analysis 311
11.4 Test Samples 311
11.4.1 Statistical Requirements 311
11.4.2 Number of Test Bearings 312
11.4.3 Test Strategy 312
11.4.4 Manufacturing Accuracy of Test Samples 312
11.5 Test Rig Design 312
11.6 Statistical Analysis of Endurance Test Data 319
11.6.1 Statistical Data Distributions 319
11.6.2 The Two-Parameter Weibull Distribution 320

11.6.2.1 Probability Functions ... 320
11.6.2.2 Mean Time between Failures ... 321
11.6.2.3 Percentiles ... 322
11.6.2.4 Graphical Representation of the Weibull Distribution ... 323
11.6.3 Estimation in Single Samples ... 324
11.6.3.1 Application of the Weibull Distribution ... 324
11.6.3.2 Point Estimation in Single Samples: Graphical Methods ... 324
11.6.3.3 Point Estimation in Single Samples: Method of Maximum Likelihood ... 326
11.6.3.4 Sudden Death Tests ... 328
16.3.3.5 Precision of Estimation: Sample Size Selection ... 329
11.6.4 Estimation in Sets of Weibull Data ... 329
11.6.4.1 Methods ... 329
11.7 Element Testing ... 331
11.7.1 Rolling Component Endurance Testers ... 331
11.7.2 Rolling–Sliding Friction Testers ... 334
11.7.2.1 Purpose ... 334
11.7.2.2 Rolling–Sliding Disk Test Rig ... 334
11.7.2.3 Ball–Disk Test Rig ... 336
11.8 Closure ... 338
References ... 340

Appendix ... 343
Index ... 345

# 1 Distribution of Internal Loading in Statically Loaded Bearings: Combined Radial, Axial, and Moment Loadings—Flexible Support of Bearing Rings

## LIST OF SYMBOLS

| Symbol | Description | Units |
|---|---|---|
| $A$ | Distance between raceway groove curvature centers | mm (in.) |
| $B$ | $f_i + f_o - 1$ | |
| $c$ | Crown drop at end of roller or raceway effective length or crown gap at other locations | mm (in.) |
| $C$ | Influence coefficient | mm/N (in./lb) |
| $D$ | Ball or roller diameter | mm (in.) |
| $D_{ij}$ | Influence coefficient to calculate nonideal roller–raceway contact deformations | |
| $d_m$ | Bearing pitch diameter | mm (in.) |
| $e$ | Eccentricity of loading | mm (in.) |
| $E$ | Modulus of elasticity | MPa (psi) |
| $f$ | $r/D$ | |
| $F$ | Applied load | N (lb) |
| $F_a$ | Friction force due to roller end–ring flange sliding motions | N (lb) |
| $h$ | Roller thrust couple moment arm | mm (in.) |
| $I$ | Ring section moment of inertia | mm$^4$ (in.$^4$) |
| $k$ | Number of laminae | |
| $K$ | Load–deflection factor, axial load–deflection factor | N/mm$^n$ (lb/in.$^n$) |
| $l$ | Roller length | mm (in.) |
| $M$ | Moment | N $\times$ mm (lb $\times$ in.) |
| $n$ | Load–deflection exponent | |
| $P_d$ | Diametral clearance | mm (in.) |
| $q$ | Load per unit length | N/mm (lb/in.) |
| $Q$ | Ball or roller–raceway normal load | N (lb) |
| $Q_a$ | Roller end–ring flange load in cylindrical roller bearing | N (lb) |
| $Q_f$ | Roller end–ring flange load in tapered roller bearing | N (lb) |

| | | |
|---|---|---|
| $r$ | Raceway groove curvature radius | mm (in.) |
| $r$ | Radius to raceway contact in tapered roller bearing | mm (in.) |
| $r_f$ | Radius from inner-ring axis to roller end–flange contact in tapered roller bearing | mm (in.) |
| $R_f$ | Radius from tapered roller axis to roller end–flange contact | mm (in.) |
| $\Re$ | Ring radius to neutral axis | mm (in.) |
| $\Re$ | Radius of locus of raceway groove curvature centers | mm (in.) |
| $s$ | Distance between loci of inner and outer raceway groove curvature centers | mm (in.) |
| $u$ | Ring radial deflection | mm (in.) |
| $U$ | Strain energy | $N \times mm$ ($lb \times in.$) |
| $Z$ | Number of balls or rollers per bearing row | |
| $\alpha$ | Mounted contact angle | rad, ° |
| $\alpha^o$ | Free contact angle | rad, ° |
| $\beta$ | $\tan^{-1} l/(d_m - D)$ | rad, ° |
| $\gamma$ | $D\cos\alpha/d_m$ | |
| $\delta$ | Deflection or contact deformation | mm (in.) |
| $\delta_1$ | Distance between inner and outer rings | mm (in.) |
| $\Delta$ | Contact deformation due to ideal normal loading | mm (in.) |
| $\Delta\psi$ | Angular spacing between rolling elements | rad, ° |
| $\zeta$ | Roller tilt angle | rad, ° |
| $\eta$ | $\tan^{-1} l/D$ | rad, ° |
| $\theta$ | Bearing misalignment angle | rad, ° |
| $\lambda$ | Lamina position | |
| $\mu$ | Coefficient of sliding friction between roller end and ring flange | |
| $\sigma$ | Normal contact stress or pressure | MPa (psi) |
| $\xi$ | Poisson's ratio | |
| $\xi$ | Roller skewing angle | rad, ° |

## 1.1 GENERAL

In most bearing applications, only applied radial, axial, or combined radial and axial loadings are considered. However, under very heavy applied loading or if shafting is hollow to minimize weight, the shaft on which the bearing is mounted may bend, causing a significant moment load on the bearing. Also, the bearing housing may be nonrigid due to design targeted at minimizing both size and weight, causing it to bend while accommodating moment loading. Such combined radial, axial, and moment loadings result in altered distribution of load among the bearing's rolling element complement. This may cause significant changes in bearing deflections, contact stresses, and fatigue endurance compared to these operating parameters associated with the simpler load distributions considered in Chapter 7 of the first volume of this handbook.

In cylindrical and tapered roller bearings, the moment loading caused by bending of the shaft results in nonuniform load per unit length along the roller–raceway contacts. Misalignment of the bearing inner ring on the shaft or outer ring in the housing also generates moment loading in the bearing, causing a nonuniform load per unit length along the roller–raceway contacts. Thus, the maximum roller–raceway contact stresses will be greater than those occurring if the contacts are loaded uniformly along their lengths. Moreover, when bearing rings are misaligned, thrust loading is induced in the rollers, causing the rollers to tilt, further exacerbating the nonuniform roller–raceway contact loading. As seen in Chapter 11 in the first volume of this

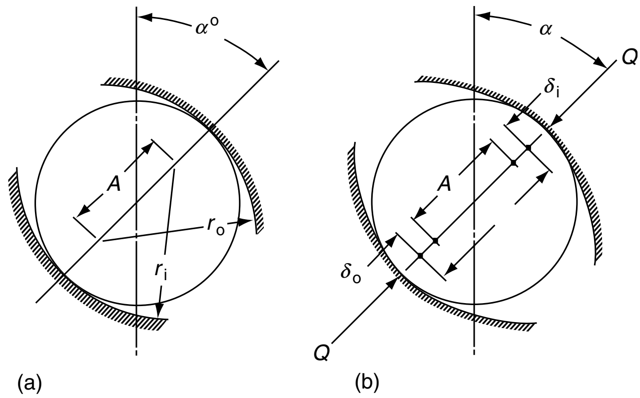


**FIGURE 1.1** (a) Ball–raceway contact before applying load; (b) ball–raceway contact after load is applied.

handbook, fatigue life is inversely proportional to approximately the ninth power of contact stress. Hence, a nonuniform roller–raceway contact loading can result in significant reduction in bearing endurance.

In this chapter, methods to determine the distribution of applied loading among the rolling elements will be established considering each of the aforementioned effects.

## 1.2 BALL BEARINGS UNDER COMBINED RADIAL, THRUST, AND MOMENT LOADS

When a ball is compressed by load $Q$, since the centers of curvature of the raceway grooves are fixed with respect to the corresponding raceways, the distance between the centers is increased by the amount of the normal approach between the raceways. From Figure 1.1, it can be seen that

$$s = A + \delta_{\mathrm{i}} + \delta_{\mathrm{o}} \tag{1.1}$$

$$\delta_{\mathrm{n}} = \delta_{\mathrm{i}} + \delta_{\mathrm{o}} = s - A \tag{1.2}$$

If a ball bearing that has a number of balls situated symmetrically about a pitch circle is subjected to a combination of radial, thrust (axial), and moment loads, the following relative displacements of inner and outer raceways may be defined:

$\delta_{\mathrm{a}}$ Relative axial displacement
$\delta_{\mathrm{r}}$ Relative radial displacement
$\theta$ Relative angular displacement

These relative displacements are shown in Figure 1.2.

Consider a rolling bearing before the application of a load. Figure 1.3 shows the positions of the loci of the centers of the inner and outer raceway groove curvature radii. It can be determined from Figure 1.4 that the locus of the centers of the inner-ring raceway groove curvature radii is expressed by

$$\Re_{\mathrm{i}} = \frac{d_{\mathrm{m}}}{2} + \left(r_{\mathrm{i}} - \frac{D}{2}\right)\cos\alpha^{\mathrm{o}} \tag{1.3}$$

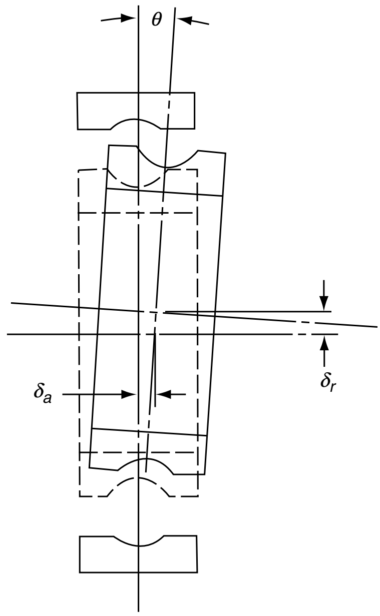


**FIGURE 1.2** Displacements of an inner ring (outer ring fixed) due to application of combined radial, axial, and moment loadings.

where $\alpha^{\mathrm{o}}$ is the free contact angle determined by bearing diametral clearance. From Figure 1.3 then

$$\Re_{\mathrm{o}} = \Re_{\mathrm{i}} - A\cos\alpha^{\mathrm{o}} \tag{1.4}$$

$$\Re_{\mathrm{i}} - \Re_{\mathrm{o}} = A\cos\alpha^{\mathrm{o}} \tag{1.5}$$

In Figure 1.3, $\psi$ is the angle between the most heavily loaded rolling element and any other rolling element. Because of symmetry $0 \leq \psi \leq \pi$.

If the outer ring of the bearing is considered fixed in space as the load is applied to the bearing, then the inner ring will be displaced and the locus of inner-ring raceway groove radii centers will also be displaced as shown in Figure 1.5. From Figure 1.5 it can be determined that $s$, the distance between the centers of curvature of the inner- and outer-ring raceway grooves at any rolling element position $\psi$, is given by

$$s = [(A\sin\alpha^{\mathrm{o}} + \delta_{\mathrm{a}} + \Re_{\mathrm{i}}\ \theta\cos\psi)^2 + (A\cos\alpha^{\mathrm{o}} + \delta_{\mathrm{r}}\cos\psi)^2]^{1/2} \tag{1.6}$$

or

$$s = A\left[\left(\sin\alpha^{\mathrm{o}} + \overline{\delta}_{\mathrm{a}} + \Re_{\mathrm{i}}\ \overline{\theta}\cos\psi\right)^2 + \left(\cos\alpha^{\mathrm{o}} + \overline{\delta}_{\mathrm{r}}\cos\psi\right)^2\right]^{1/2} \tag{1.7}$$

where

$$\overline{\delta}_{\mathrm{a}} = \frac{\delta_{\mathrm{a}}}{A} \tag{1.8}$$

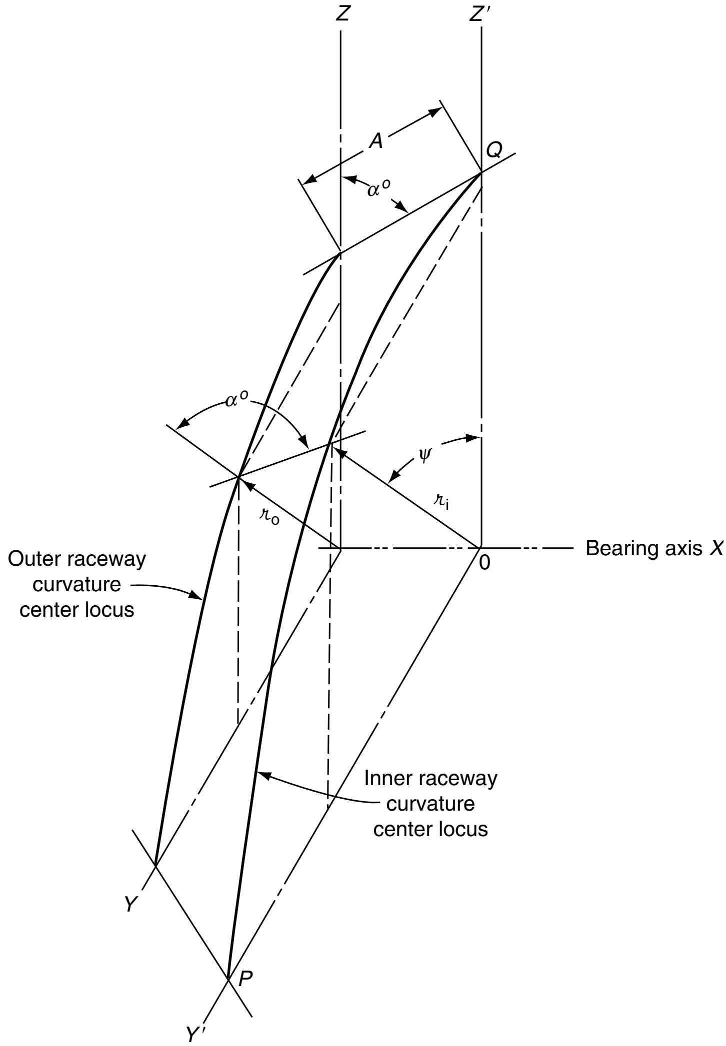


**FIGURE 1.3** Loci of raceway groove curvature radii centers before applying load. (From Jones, A., *Analysis of Stresses and Deflections*, New Departure Engineering Data, Bristol, CT, 1946.)

$$\bar{\delta}_r = \frac{\delta_r}{A} \tag{1.9}$$

$$\bar{\theta} = \frac{\theta}{A} \tag{1.10}$$

Substituting Equation 1.7 into Equation 1.2 yields

$$\delta_n = A\left\{\left[\left(\sin\alpha^o + \bar{\delta}_a + \Re_i\,\bar{\theta}\cos\psi\right)^2 + \left(\cos\alpha^o + \bar{\delta}_r\cos\psi\right)^2\right]^{1/2} - 1\right\} \tag{1.11}$$

From Chapter 7 of the first volume of this book, the load vs. deformation relationship for a rolling element–raceway contact is given by

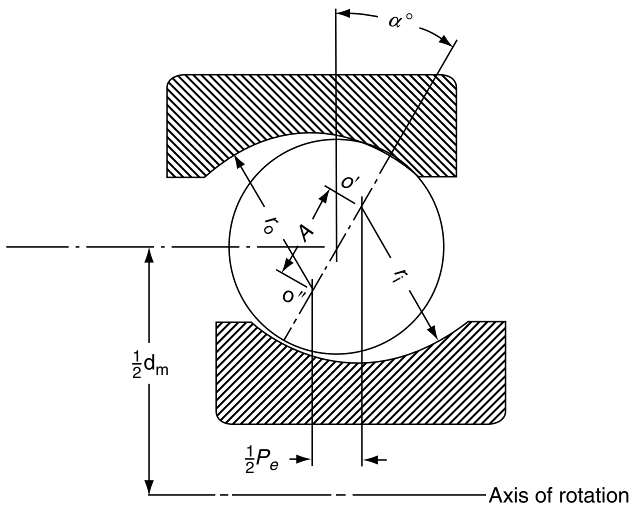


**FIGURE 1.4** Radial ball bearing showing ball–raceway contact due to axial shift of inner and outer rings.

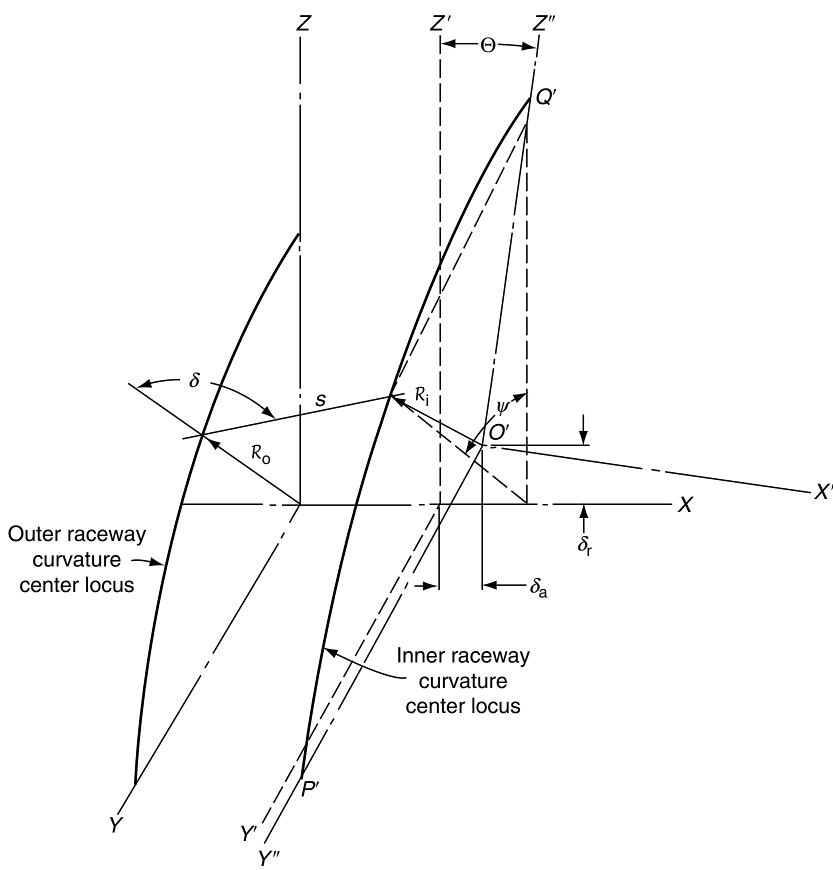


**FIGURE 1.5** Loci of raceway groove curvature radii centers after displacement (From Jones, A., *Analysis of Stresses and Deflections*, New Departure Engineering Data, Bristol, CT, 1946.)

$$Q = K_n \delta^n \tag{1.12}$$

In Equation 1.12, exponent $n = 3/2$ for ball bearings and 10/9 for roller bearings. Substitution of Equation 1.11 into Equation 1.12 and using the former exponent gives

$$Q = K_n A^{1.5} \left\{ \left[ \left( \sin \alpha^o + \bar{\delta}_a + \Re_i \bar{\theta} \cos \psi \right)^2 + \left( \cos \alpha^o + \bar{\delta}_r \cos \psi \right)^2 \right]^{1/2} - 1 \right\}^{1.5} \tag{1.13}$$

At any ball azimuth position $\psi$, the operating contact angle is $\alpha$. This angle can be determined from

$$\sin \alpha = \frac{\sin \alpha^o + \bar{\delta}_a + \Re_i \bar{\theta} \cos \psi}{\left[ \left( \sin \alpha^o + \bar{\delta}_a + \Re_i \bar{\theta} \cos \psi \right)^2 + \left( \cos \alpha^o + \bar{\delta}_r \cos \psi \right)^2 \right]^{1/2}} \tag{1.14}$$

or

$$\cos \alpha = \frac{\cos \alpha^o + \bar{\delta}_r \cos \psi}{\left[ \left( \sin \alpha^o + \bar{\delta}_a + \Re_i \bar{\theta} \cos \psi \right)^2 + \left( \cos \alpha^o + \bar{\delta}_r \cos \psi \right)^2 \right]^{1/2}} \tag{1.15}$$

Equation 1.12 describes the normal load on the raceway acting through the contact angle. This normal load may be resolved into axial and radial components as follows:

$$Q_a = Q \sin \alpha \tag{1.16}$$

$$Q_r = Q \cos \psi \cos \alpha \tag{1.17}$$

If the radial and thrust loads applied to the bearing are $F_r$ and $F_a$, respectively, then for static equilibrium to exist

$$F_a = \sum_{\psi = 0}^{\psi = \pm\pi} Q_\psi \sin \alpha \tag{1.18}$$

$$F_r = \sum_{\psi = 0}^{\psi = \pm\pi} Q_\psi \cos \psi \cos \alpha \tag{1.19}$$

Additionally, each of the thrust components produce a moment about the $Y$-axis such that

$$M_\psi = \frac{d_m}{2} Q_\psi \cos \psi \sin \alpha \tag{1.20}$$

For static equilibrium, the applied moment $M$ about the $Y$-axis must equal the sum of the moments of each rolling element about the $Y$-axis (in the case of load symmetry, rolling element thrust component moments about the $Z$-axis are self-equilibrating).

$$M = \frac{d_m}{2} \sum_{\psi = 0}^{\psi = \pm\pi} Q_\psi \cos \psi \sin \alpha \tag{1.21}$$

Combining Equation 1.13, Equation 1.16, and Equation 1.18 yields

$$F_a - K_n A^{1.5} \sum_{\psi=0}^{\psi=\pm\pi} \frac{\left\{\left[\left(\sin\alpha^o + \bar{\delta}_a + \Re_i \bar{\theta}\cos\psi\right)^2 + \left(\cos\alpha^o + \bar{\delta}_r\cos\psi\right)^2\right]^{1/2} - 1\right\}^{1.5} \left(\sin\alpha^o + \bar{\delta}_a + \Re_i \bar{\theta}\cos\psi\right)}{\left[\left(\sin\alpha^o + \bar{\delta}_a + \Re_i \bar{\theta}\cos\psi\right)^2 + \left(\cos\alpha^o + \bar{\delta}_r\cos\psi\right)^2\right]^{1/2}} = 0 \tag{1.22}$$

$$F_r - K_n A^{1.5} \sum_{\psi=0}^{\psi=\pm\pi} \frac{\left\{\left[\left(\sin\alpha^o + \bar{\delta}_a + \Re_i \bar{\theta}\cos\psi\right)^2 + \left(\cos\alpha^o + \bar{\delta}_r\cos\psi\right)^2\right]^{1/2} - 1\right\}^{1.5} \left(\cos\alpha^o + \bar{\delta}_r\cos\psi\right)\cos\psi}{\left[\left(\sin\alpha^o + \bar{\delta}_a + \Re_i \bar{\theta}\cos\psi\right)^2 + \left(\cos\alpha^o + \bar{\delta}_r\cos\psi\right)^2\right]^{1/2}} = 0 \tag{1.23}$$

$$M - \frac{d_m}{2} K_n A^{1.5} \sum_{\psi=0}^{\psi=\pm\pi} \frac{\left\{\left[\left(\sin\alpha^o + \bar{\delta}_a + \Re_i \bar{\theta}\cos\psi\right)^2 + \left(\cos\alpha^o + \bar{\delta}_r\cos\psi\right)^2\right]^{1/2} - 1\right\}^{1.5} \left(\sin\alpha^o + \bar{\delta}_a + \Re_i \bar{\theta}\cos\psi\right)\cos\psi}{\left[\left(\sin\alpha^o + \bar{\delta}_a + \Re_i \bar{\theta}\cos\psi\right)^2 + \left(\cos\alpha^o + \bar{\delta}_r\cos\psi\right)^2\right]^{1/2}} = 0 \tag{1.24}$$

These equations were developed by Jones [1].

Equation 1.22 through Equation 1.24 are simultaneous nonlinear equations with unknowns $\delta_a$, $\delta_r$, and $\theta$. They may be solved by numerical methods; for example, the Newton–Raphson method. Having obtained $\delta_a$, $\delta_r$, and $\theta$, the maximum ball load may be obtained from Equation 1.13 for $\psi = 0$.

$$Q_{max} = K_n A^{1.5} \left\{\left[\left(\sin\alpha^o + \bar{\delta}_a + \Re_i \bar{\theta}\right)^2 + \left(\cos\alpha^o + \bar{\delta}_r\right)^2\right]^{1/2} - 1\right\}^{1.5} \tag{1.25}$$

Solution of the indicated equations generally necessitates the use of a digital computer.

## 1.3 MISALIGNMENT OF RADIAL ROLLER BEARINGS

Although it is undesirable, radial cylindrical roller bearings and tapered roller bearings can support to a small extent the moment loading due to misalignment. The various types of misalignment are illustrated in Figure 1.6. Spherical roller bearings are designed to exclude moment loads from acting on the bearings and therefore are not included in this discussion. Figure 1.7 illustrates the misalignment of the inner ring of a cylindrical roller bearing relative to the outer ring.

To commence the analysis, it is assumed that any roller–raceway contact can be divided into a number of "slices" or laminae situated in planes parallel to the radial plane of the bearing. It is also assumed that shear effects between these laminae can be neglected owing to the small magnitudes of the contact deformations that develop. (Only contact deformations are considered.)

### 1.3.1 Components of Deformation

In a misaligned cylindrical roller bearing subjected to radial load, at each lamina in a crowned roller–raceway contact, the deformation may be considered to be composed of three components: (1) $\Delta_{mj}$ due to the radial load at the roller azimuth location $j$, (2) $c_\lambda$ due to the crown drop at lamina $\lambda$, and (3) the deformation due to bearing misalignment and

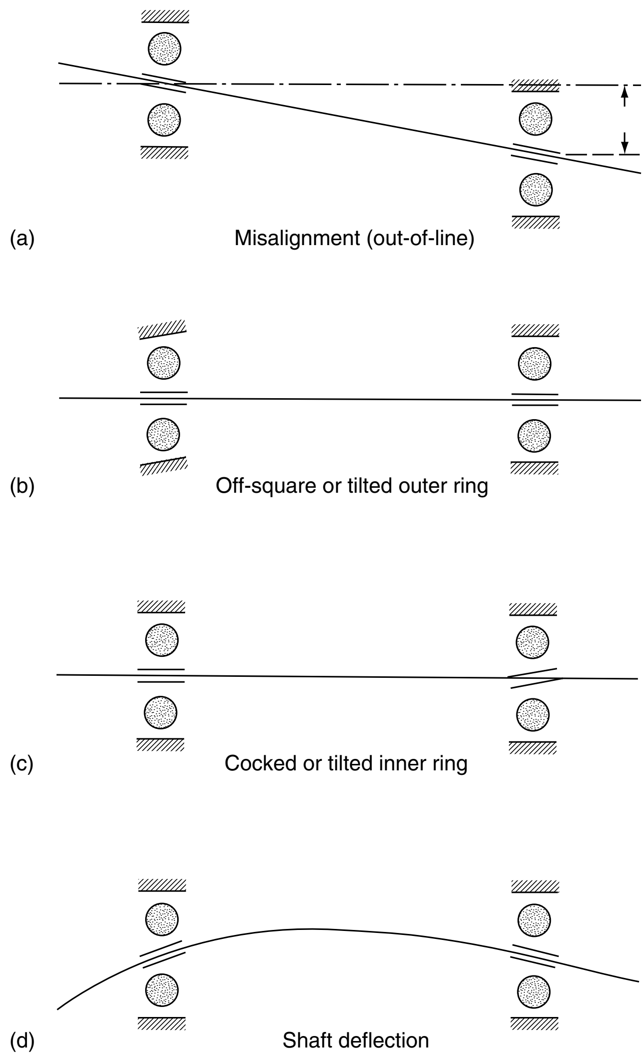


**FIGURE 1.6** Types of misalignments.

roller tilt at the roller azimuth location *j*. These components are shown schematically in Figure 1.8.

The component due to radial load is the only contact deformation component considered in the simplified analytical methods presented in Chapter 7 of the first volume of this book. It needs no further explanation here.

#### 1.3.1.1 Crowning

As stated previously, crowning of rollers and raceways is accomplished to avoid edge loading that can result in early fatigue failure of the rolling components. It may be accomplished in various forms. The simplest of these is the full circular profile crown illustrated in Figure 1.9. The rollers in most spherical roller bearings may be considered fully crowned whether of symmetrical contour (barrel-shaped) or of asymmetrical contour. In the latter case, the crown is offset from the roller mid-length point. Full crowning may also be applied to raceways as

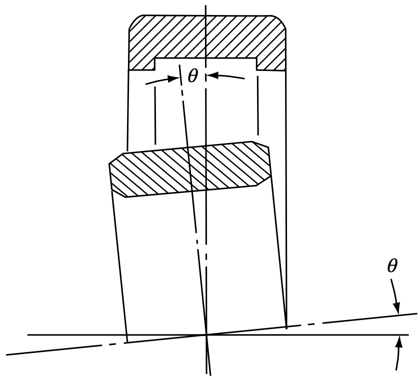


**FIGURE 1.7** Misalignment of cylindrical roller bearing rings.

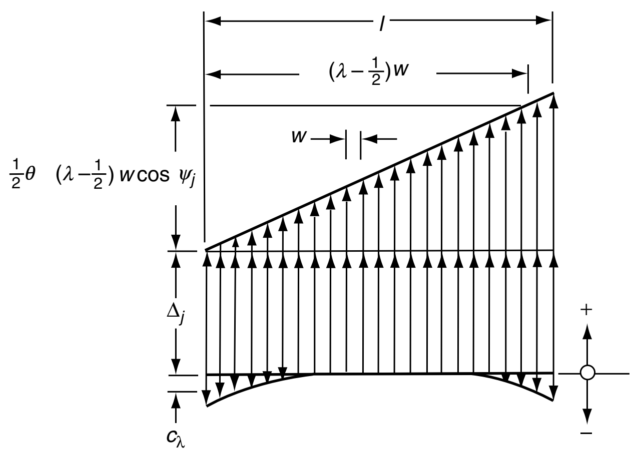


**FIGURE 1.8** Components of roller–raceway contact deformation due to radial load, misalignment, and crowning.

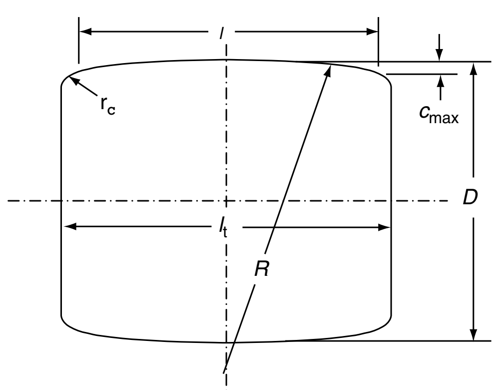


**FIGURE 1.9** Schematic diagram of cylindrical roller with full circular profile crown.

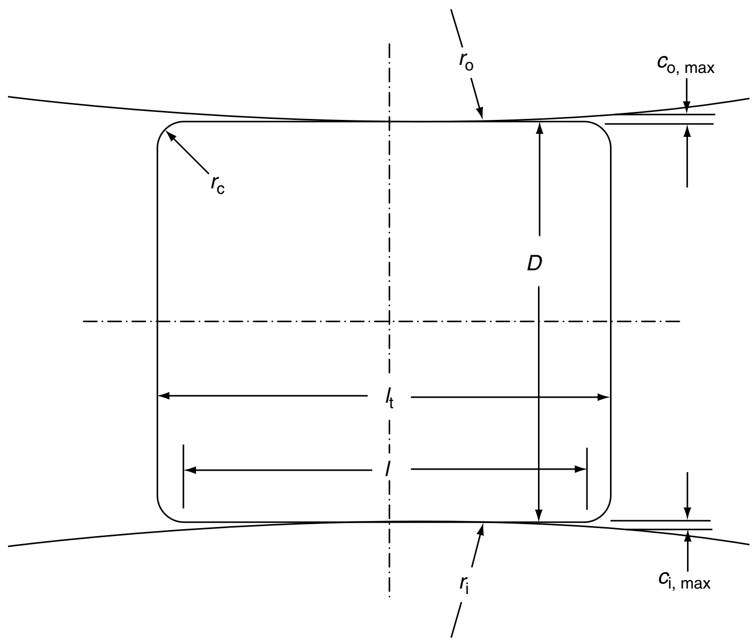


**FIGURE 1.10** Schematic diagram of uncrowned (straight profile) cylindrical roller contacting inner and outer raceways, each with a full circular profile crown.

shown in Figure 1.10. This is commonly used in tapered roller bearings where often both the cone and cup raceways are crowned, and the rollers are not crowned.

Most cylindrical roller bearings employ rollers that are crowned only over a portion of the roller contour; the remaining portion is cylindrical (the contour is sometimes called flat or straight). A partially crowned cylindrical roller is illustrated in Figure 1.11.

From Figure 1.8, it can be seen that crown drop or crown gap $c_\lambda$ at a selected lamina is considered as a negative deformation; that is, no roller–raceway loading can occur at a lamina until $c_\lambda$ is overcome by the radial or the misalignment deformation. For both the fully crowned or partially crowned rollers that have circular profiles, Equation 1.26 defines $c_\lambda$ in terms of the roller and crown dimensions, where $1 \leq \lambda \leq k$.

$$c_\lambda = \left\{ \begin{array}{ll} c_{\max}\left[\dfrac{\left(\frac{2\lambda-1}{k}-1\right)^2-\left(\frac{l_s}{l}\right)^2}{1-\frac{l_s}{l}}\right] & \left(\dfrac{2\lambda-1}{k}-1\right)^2-\left(\dfrac{l_s}{l}\right)^2>0 \\ 0 & \left(\dfrac{2\lambda-1}{k}-1\right)^2-\left(\dfrac{l_s}{l}\right)^2\leq 0 \end{array} \right\} \tag{1.26}$$

For rollers with circular profile partial crowns, blending between the straight and crowned portions of the profile is necessary to minimize stress concentrations and the resulting reduced fatigue life. To avoid such stress concentrations, in lieu of a circular profile, a tangential profile might be used. In this case, the crown radius would be variable, and the crown gap at each lamina $k$ would be calculated using

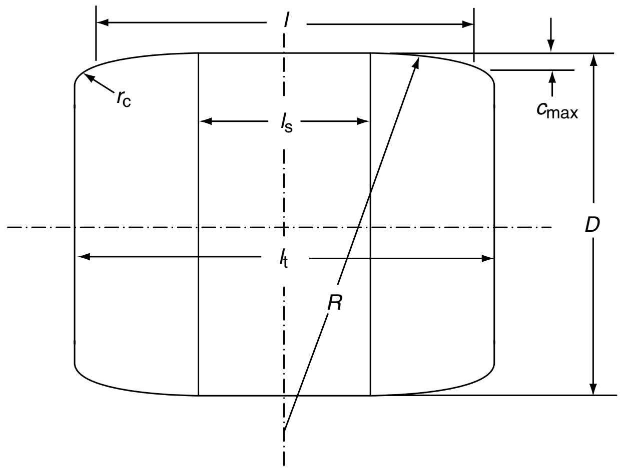


**FIGURE 1.11** Schematic diagram of a partially crowned cylindrical roller.

$$c_\lambda = \begin{cases} c_{\max}\left[\dfrac{\left|\frac{2\lambda-1}{k}-1\right|-\frac{l_s}{l}}{1-\frac{l_s}{l}}\right]^2 & \left|\frac{2\lambda-1}{k}-1\right|-\frac{l_s}{l}>0 \\ 0 & \left|\frac{2\lambda-1}{k}-1\right|-\frac{l_s}{l}\le 0 \end{cases} \tag{1.27}$$

To minimize edge loading, Lundberg and sjövall [2] devised a fully crowned roller having a logarithmic profile. The crown gap at each lamina $k$ is calculated using

$$c_\lambda = 0.2 \cdot ln\left[\frac{1}{1.0067-\left(\frac{2\lambda-1}{k}-1\right)^2}\right] \tag{1.28}$$

Subsequently, Reussner [3] developed another logarithmic profile crown believed to be more effective. The crown gap at each lamina $k$ for the Reussner crown profile is given by

$$c_\lambda = 2\times10^{-4}\Sigma\rho w^2k^2 \cdot \ln\left[\frac{1}{1-\left(\frac{2\lambda-1}{k}-1\right)^6}\right] \tag{1.29}$$

It is possible to combine roller crowning and raceway crowning. In this case, the crown gap at each lamina $k$ would be calculated as the sum of the crown gaps for the roller and raceway as follows:

$$c_{m\lambda} = c_{R\lambda} + c_{m\lambda} \tag{1.30}$$

In the above equation, subscript R refers to the roller and m to the raceway (m = i or m = o).

For the bearing misalignment $\theta$ shown in Figure 1.7, the effective misalignment at the azimuth location of the roller $\psi_j$ is $\pm 1/2\theta$ cos $\psi_j$. The plus sign pertains to $0 \le \psi_j \le \pi/2$; the minus sign pertains to $\pi/2 \le \psi_j \le \pi$ (assuming symmetry of loading about the 0–$\pi$ diameter). Therefore, the total roller–raceway deformation at roller location $j$ and lamina $\lambda$ is given by

$$\delta_{\lambda j} = \Delta_j \pm \frac{\theta}{2}\left(\lambda - \frac{1}{2}\right) w \cos\psi_j - c_\lambda \tag{1.31}$$

### 1.3.2 Load on a Roller–Raceway Contact Lamina

In Chapter 6 of the first volume of this book, the following equations were given to describe the deformation vs. load for a roller–raceway contact:

$$\delta = \frac{2Q\left(1-\xi^2\right)}{\pi El} \ln\left[\frac{\pi El^2}{Q\left(1-\xi^2\right)(1 \mp \gamma)}\right] \tag{1.32}$$

$$\delta = 3.84 \times 10^{-5} \frac{Q^{0.9}}{l^{0.8}} \tag{1.33}$$

Equation 1.32 was developed by Lundberg and Sjövall [2] for an ideal line contact. In Equation 1.32, $\gamma = D\cos\alpha/d_\mathrm{m}$, $E$ is the modulus of elasticity, and $\xi$ is Poisson's ratio. Equation 1.33 was developed empirically by Palmgren [4] from laboratory test data and pertains to the contact of a crowned roller on a raceway. While the load–deformation characteristic of an individual contact lamina may be described using either equation, the latter is applied here as the solution of a transcendental equation leads to force and moment equilibrium equations of greater complexity. Considering that the contact is divided into $k$ laminae, each lamina of width $w$, the contact length is $kw$. Letting $q = Q/l$, Equation 1.33 becomes

$$\delta = 3.84 \times 10^{-5} q^{0.9} (kw)^{0.1} \tag{1.34}$$

Rearranging the above equation to define $q$ yields

$$q = \frac{\delta^{1.11}}{1.24 \times 10^{-5}\ (kw)^{0.11}} \tag{1.35}$$

Equation 1.35 does not consider edge stresses; however, because these obtain only over very small areas, they can be neglected with little loss of accuracy when considering equilibrium of loading. Substitution of Equation 1.31 into Equation 1.35 gives

$$q_{\lambda j} = \frac{\left[\Delta_j \pm \theta\left(\lambda - \frac{1}{2}\right) w \cos\psi_j - c_\lambda\right]^{1.11}}{1.24 \times 10^{-5} (k_j w)^{0.11}} \tag{1.36}$$

Depending on the degree of loading and misalignment, all laminae in every contact may not be loaded; in Equation 1.36, $k_j$ is the number of laminae under load at roller location $j$. Total roller loading is given by

$$Q_j = \frac{w^{0.89}}{1.24 \times 10^{-5} k_j^{0.11}} \sum_{\lambda=1}^{\lambda=k_j} \left[\Delta_j \pm \frac{1}{2}\theta\left(\lambda - \frac{1}{2}\right) w \cos\psi_j - c_\lambda\right]^{1.11} \tag{1.37}$$

### 1.3.3 Equations of Static Equilibrium

To determine the individual roller loading, it is necessary to satisfy the requirements of static equilibrium. Hence, for an applied radial load,

$$\frac{F_r}{2} - \sum_{j=1}^{j=Z/2+1} \tau_j Q_j \cos\psi_j = 0 \quad \begin{array}{ll} \tau_j = 0.5; & \psi_j = 0, \pi \\ \tau_j = 1; & \psi_j \neq 0, \pi \end{array} \tag{1.38}$$

Substituting Equation 1.37 into Equation 1.38 yields

$$\frac{0.62 \times 10^{-5} F_r}{w^{0.89}} - \sum_{j=1}^{j=Z/2+1} \frac{\tau_j \cos\psi_j}{k_j^{0.11}} \sum_{\lambda=1}^{\lambda=k_j} \left[\Delta_j \pm \frac{1}{2}\theta\left(\lambda - \frac{1}{2}\right) w \cos\psi_j - c_\lambda\right]^{1.11} = 0 \tag{1.39}$$

For an applied coplanar misaligning moment load, the equilibrium condition to be satisfied is

$$\frac{\mathfrak{M}}{2} - \sum_{j=1}^{j=Z/2+1} \tau_j Q_j e_j \cos\psi_j = 0 \quad \begin{array}{ll} \tau_j = 0.5; & \psi_j = 0, \pi \\ \tau_j = 1; & \psi_j \neq 0, \pi \end{array} \tag{1.40}$$

where $e_j$ is the eccentricity of loading at each roller location. $e_j$, which is illustrated in Figure 1.12, is given by

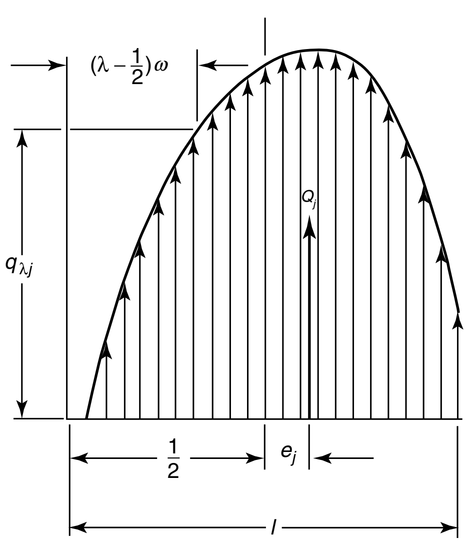


**FIGURE 1.12** Load distribution for a misaligned crowned roller showing eccentricity of loading.

$$e_j = \frac{\sum_{\lambda=1}^{\lambda=k_j} q_{\lambda j}\left(\lambda - \frac{1}{2}\right)w}{\sum_{\lambda=1}^{\lambda=k_j} q_{\lambda j}} - \frac{l}{2} \quad j = 3, \qquad \frac{Z}{2} + 3 \tag{1.41}$$

Hence,

$$\begin{aligned} &\frac{0.62 \times 10^{-5}\mathfrak{M}}{w^{0.89}} - \sum_{j=1}^{j=Z/2+1} \frac{\tau_j \cos\psi_j}{k_j^{0.11}} \\ &\times \left\{ \sum_{\lambda=1}^{\lambda=k_j} \left[\Delta_j \pm \frac{1}{2}\theta\left(\lambda - \frac{1}{2}\right) w\cos\psi_j - c_j\right]^{1.11} \left(\lambda - \frac{1}{2}\right) w \right. \\ &\left. - \frac{l}{2} \sum_{\lambda=1}^{\lambda=k_j} \left[\Delta_j \pm \frac{1}{2}\theta\left(\lambda - \frac{1}{2}\right) w\cos\psi_j - c_\lambda\right]^{1.11} \right\} = 0 \end{aligned} \tag{1.42}$$

### 1.3.4 Deflection Equations

The remaining equations to be established are the radial deflection relationships. It is necessary here to determine the relative radial movement of the rings caused by the misalignment as well as that owing to radial loading. To assist in the first determination, Figure 1.13 shows schematically an inner ring–roller assembly misaligned with respect to the outer ring. From this sketch, it is evident that one half of the roller included angle is described by

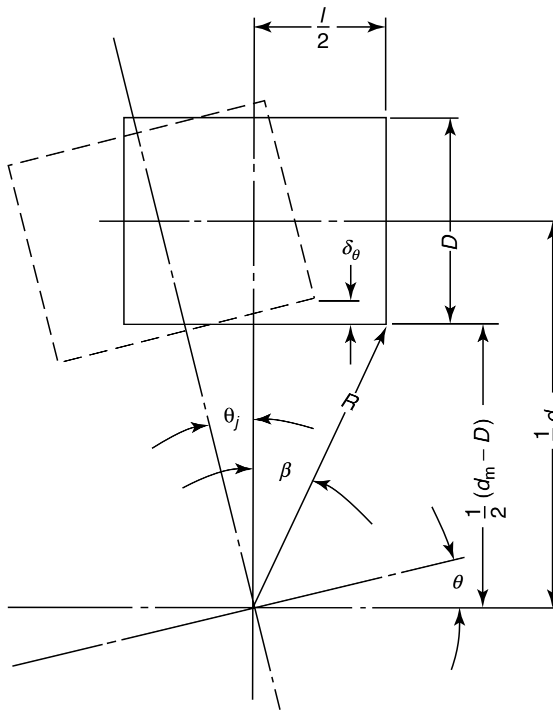


**FIGURE 1.13** Schematic diagram of misaligned roller–inner ring assembly showing interference with outer ring.

$$\beta = \tan^{-1}\frac{l}{d_{\mathrm{m}} - D} \tag{1.43}$$

and

$$\sin\beta = \frac{l}{[(d_{\mathrm{m}} - D)^2 + l^2]^{1/2}} \tag{1.44}$$

The maximum radial interference between a roller and the outer ring owing to misalignment is given by

$$\delta_\theta = R\cos(\beta - \theta_j) - R\cos\beta \tag{1.45}$$

where

$$R = 0.5 \times [(d_{\mathrm{m}} - D)^2 + l^2]^{1/2} \tag{1.46}$$

In developing Equation 1.45 and Equation 1.46, the effect of crown drop was investigated and found to be negligible.

Expanding Equation 1.46 in terms of the trigonometric identity further yields

$$\delta_\theta = R(\cos\beta\,\cos\theta_j + \sin\beta\,\sin\theta_j - \cos\beta) \tag{1.47}$$

As $\theta_j$ is small, $\cos\theta_j \to 1$, and $\sin\theta_j \to \theta_j$. Moreover, $\theta_j = \pm\theta\cos\psi_j$ and $\sin\beta = l/2R$; therefore,

$$\delta_\theta = \pm\tfrac{1}{2}\,l\theta\cos\psi_j \tag{1.48}$$

The shift of the inner-ring center relative to the outer-ring center owing to radial loading and clearance, and the subsequent relative radial movement at any roller location are shown in Figure 1.14. The sum of the relative radial movement of the rings at each roller angular location minus the clearance is equal to the sum of the inner and outer raceway maximum contact deformations at the same angular location. Stating this relationship in equation format:

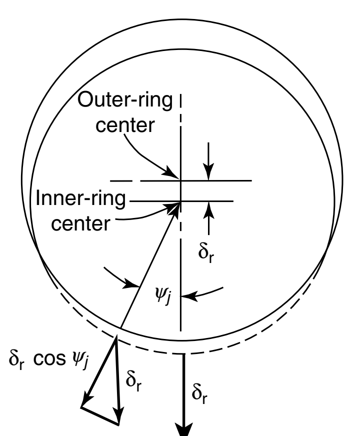


**FIGURE 1.14** Displacement of ring centers caused by radial loading showing relative radial movement.

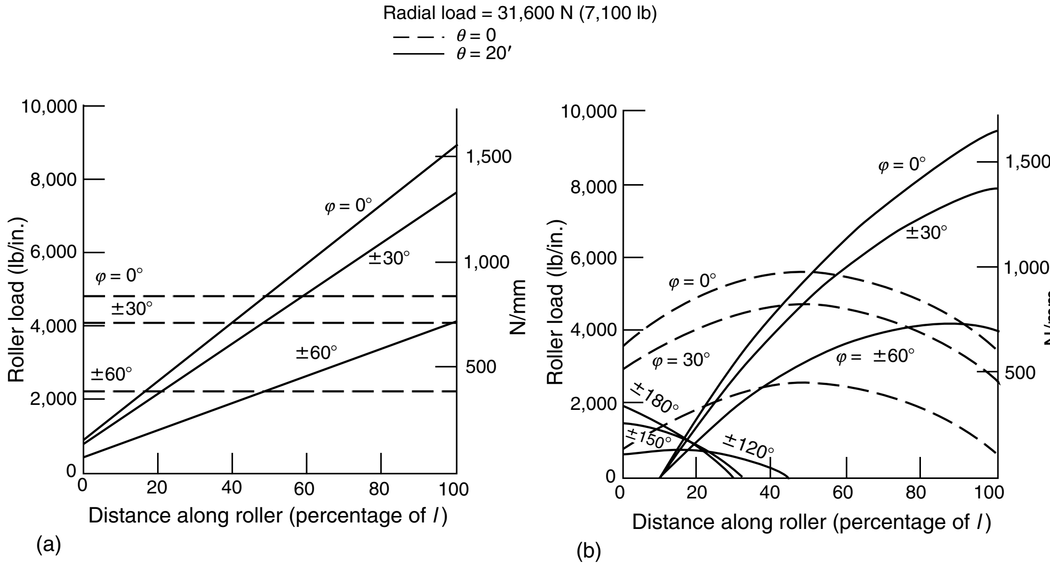


**FIGURE 1.15** Roller loading vs. axial and circumferential location—309 cylindrical roller bearing: (a) ideally crowned rollers; (b) fully crowned rollers.

$$\left[\delta_r \pm \frac{1}{2}l\theta\right]\cos\psi_j - \frac{P_d}{2} - 2\left[\Delta_j \pm \frac{1}{2}\theta\left(\lambda - \frac{1}{2}\right)w\cos\psi_j - c_\lambda\right]_{\max} = 0 \qquad (1.49)$$

Equation 1.39, Equation 1.42, and Equation 1.49 constitute a set of $Z/2+3$ simultaneous nonlinear equations that can be solved for $\delta_r$, $\theta$, and $\Delta_j$ using numerical analysis techniques. Thereafter, the variation of roller load per unit length, and subsequently the roller load, may be determined for each roller location using Equation 1.36 and Equation 1.37, respectively.

Using this method of digital computation, Harris [5] analyzed a 309 cylindrical roller bearing having the following dimensions and loading:

| | |
|---|---|
| Number of rollers | 12 |
| Roller effective length | 12.6 mm (0.496 in.) |
| Roller straight lengths | 4.78, 7.770, 12.6 mm |
| Roller crown radius | 1,245 mm (49 in.) |
| Roller diameter | 14 mm (0.551 in.) |
| Bearing pitch diameter | 72.39 mm (2.85 in.) |
| Applied radial load | 31,600 N (7,100 lb) |

For these conditions, Figure 1.15 shows the loading on various rollers for the bearing with ideally crowned rollers ($l_s = 12.6$ mm [0.496 in.]) and with fully crowned rollers ($l_s = 0$).

Figure 1.16 shows the effect of roller crowning on bearing radial deflection as a function of misalignment.

## 1.4 THRUST LOADING OF RADIAL CYLINDRICAL ROLLER BEARINGS

When radial cylindrical roller bearings have fixed flanges on both inner and outer rings, they can carry some thrust load in addition to radial load. The greater the amount of radial load applied, the more is the thrust load that can be carried. As shown by Harris [6] and seen in Figure 1.17, the thrust load causes each roller to tilt an amount $\zeta_j$.

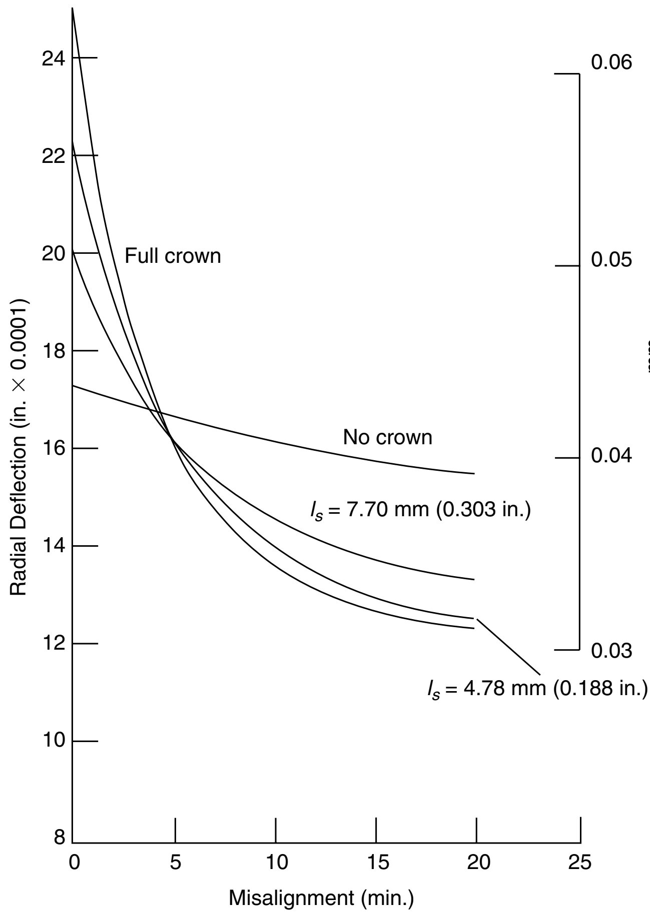


**FIGURE 1.16** Roller deflection vs. misalignment and crowning—309 cylindrical roller bearing at 31,600 N (7,100 lb) radial load.

Again, it is assumed that a roller–raceway contact can be subdivided into laminae in planes parallel to the radial plane of the bearing. When a radial cylindrical roller bearing is subjected to applied thrust load, the inner ring shifts axially relative to the outer ring.

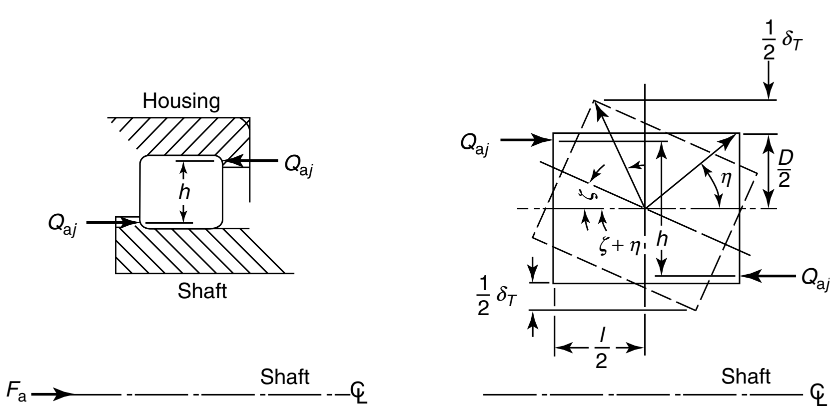


**FIGURE 1.17** Thrust couple, roller tilting, and interference owing to applied thrust load.

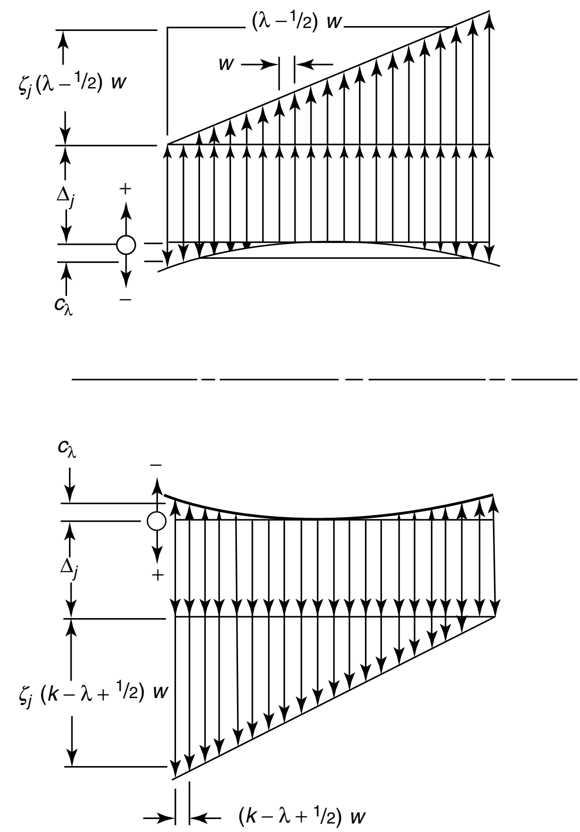


**FIGURE 1.18** Components of roller–raceway deflection at opposing raceways due to radial load, thrust load, and crowning.

Assuming deflections owing to roller end–flange contacts are negligible, the interference at any axial location (lamina) is

$$\delta_{\lambda j} = \Delta_j + \zeta_j\left(\lambda - \frac{1}{2}\right)w - c_\lambda, \quad \lambda = 1, k_j \tag{1.50}$$

where $c_\lambda$ is given by Equation 1.26 through Equation 1.30. Figure 1.18 illustrates the component deflections in Equation 1.50. Substituting Equation 1.50 into Equation 1.35 yields

$$q_{\lambda j} = \frac{\left[\Delta_j + \zeta_j\left(\lambda - \frac{1}{2}\right)w - c_\lambda\right]^{1.11}}{1.24 \times 10^{-5}(k_j w)^{0.11}} \tag{1.51}$$

and at any azimuth $\psi_j$, the total roller loading is

$$Q_j = \frac{w^{0.89}}{1.24 \times 10^{-5}k_j^{0.11}} \sum_{\lambda=1}^{\lambda=k_j} \left[\Delta_j + \zeta_j\left(\lambda - \frac{1}{2}\right)w - c_\lambda\right]^{1.11} \tag{1.52}$$

### 1.4.1 Equilibrium Equations

To determine roller loading, it is necessary to satisfy static equilibrium requirements. Hence, for applied radial load

$$\frac{F_r}{2} - \sum_{j=1}^{j=Z/2+1} \tau_j Q_j \cos\psi_j = 0 \quad \begin{array}{ll} \tau_j = 0.5; & \psi_j = 0, \pi \\ \tau_j = 1; & \psi_j \neq 0, \pi \end{array} \tag{1.53}$$

Substituting Equation 1.52 into Equation 1.53 yields

$$\frac{0.62 \times 10^{-5} F_r}{w^{0.89}} - \sum_{j=1}^{j=Z/2+1} \frac{\tau_j \cos\psi_j}{k_j^{0.11}} \sum_{\lambda=1}^{\lambda=k_j} \left[\Delta_j + \zeta_j\left(\lambda - \frac{1}{2}\right)w - c_\lambda\right]^{1.11} = 0 \tag{1.54}$$

For an applied centric thrust load, the equilibrium condition to be satisfied is

$$\frac{F_a}{2} - \sum_{j=1}^{j=Z/2+1} \tau_j Q_{aj} = 0 \tag{1.55}$$

At each roller location, the thrust couple is balanced by a radial load couple caused by the skewed axial load distribution. Thus, $hQ_{aj} = 2Q_j e_j$ and

$$\frac{F_a}{2} - \frac{2}{h} \sum_{j=1}^{j=Z/2+1} \tau_j Q_j e_j = 0 \quad \begin{array}{ll} \tau_j = 0.5; & \psi_j = 0, \pi \\ \tau_j = 1; & \psi_j \neq 0, \pi \end{array} \tag{1.56}$$

where $e_j$ is the eccentricity of loading indicated in Figure 1.12 and defined by

$$e_j = \frac{\sum_{\lambda=1}^{\lambda=k_j} q_{\lambda j}\left(\lambda - \frac{1}{2}\right)w}{\sum_{\lambda=1}^{\lambda=k_j} q_{\lambda j}} - \frac{l}{2} \tag{1.57}$$

Substitution of Equation 1.52 and Equation 1.57 into Equation 1.56 yields

$$\begin{aligned} &\frac{0.31 \times 10^{-5} F_a}{w^{0.89}} - \sum_{j=1}^{j=Z/2+1} \frac{\tau_j}{k_j^{0.11}} \\ &\quad \times \left\{ \sum_{\lambda=1}^{\lambda=k_j} \left[\Delta_j \pm \zeta_j\left(\lambda - \frac{1}{2}\right)w - c_\lambda\right]^{1.11} \left(\lambda - \frac{1}{2}\right)w - \frac{l}{2} \right. \\ &\quad \left. \times \sum_{\lambda=1}^{\lambda=k_j} \left[\Delta_j \pm \zeta_j\left(\lambda - \frac{1}{2}\right)w - c_\lambda\right]^{1.11} \right\} = 0 \quad \begin{array}{ll} \tau_j = \frac{1}{2}; & \psi_j = 0, \pi \\ \tau_j = 1; & \psi_j \neq 0, \pi \end{array} \end{aligned} \tag{1.58}$$